



RESEARCH ARTICLE | OCTOBER 09 2024

## Identification and classification of clusters of dipolar colloids in an external field

Katherine Skipper; Fergus J. Moore; C. Patrick Royall  



*J. Chem. Phys.* 161, 144308 (2024)

<https://doi.org/10.1063/5.0225759>



### Articles You May Be Interested In

Energy landscapes for clusters of hexapeptides

*J. Chem. Phys.* (August 2024)

The alchemical energy landscape for a pentameric cluster

*J. Chem. Phys.* (January 2020)

Global optimization of bimetallic cluster structures. I. Size-mismatched Ag–Cu, Ag–Ni, and Au–Cu systems

*J. Chem. Phys.* (May 2005)



The Journal of Chemical Physics

## Special Topics Open for Submissions

[Learn More](#)

# Identification and classification of clusters of dipolar colloids in an external field

Cite as: *J. Chem. Phys.* **161**, 144308 (2024); doi: [10.1063/5.0225759](https://doi.org/10.1063/5.0225759)

Submitted: 26 June 2024 • Accepted: 19 September 2024 •

Published Online: 9 October 2024



View Online



Export Citation



CrossMark

Katherine Skipper,<sup>1,2</sup> Fergus J. Moore,<sup>1,2</sup> and C. Patrick Royall<sup>1,2,3,4,a)</sup> 

## AFFILIATIONS

<sup>1</sup>H.H. Wills Physics Laboratory, Tyndall Avenue, Bristol BS8 1TL, United Kingdom

<sup>2</sup>Centre for Nanoscience and Quantum Information, Tyndall Avenue, Bristol BS8 1FD, United Kingdom

<sup>3</sup>Gulliver UMR CNRS 7083, ESPCI Paris, Université PSL, 75005 Paris, France

<sup>4</sup>School of Chemistry, Cantock's Close, University of Bristol, Bristol BS8 1TS, United Kingdom

<sup>a)</sup>Author to whom correspondence should be addressed: [paddy.royall@espci.psl.eu](mailto:paddy.royall@espci.psl.eu)

## ABSTRACT

Colloids can acquire a dipolar interaction in the presence of an external AC electric field. At high field strength, the particles form strings in the field direction. However, at weaker field strength, competition with isotropic interactions is expected. One means to investigate this interplay between dipolar and isotropic interactions is to consider clusters of such particles. Therefore, we have identified, using the GMIN basin-hopping tool, a rich library of lowest energy clusters of a dipolar colloidal system, where the dipole orientation is fixed to lie along the  $z$  axis and the dipole strength is varied for  $m$ -membered clusters of  $7 \leq m \leq 13$ . In the regime where the isotropic and dipolar interactions are comparable, we find elongated polytetrahedral, octahedral, and spiral clusters as well as a set of non-rigid clusters, which emerge close to the transition to strings. We further implement a search algorithm that identifies these minimum energy clusters in bulk systems using the *topological cluster classification* [*J. Chem. Phys.* **139** 234506 (2013)]. We demonstrate this methodology with computer simulations, which show instances of these clusters as a function of dipole strength.

Published under an exclusive license by AIP Publishing. <https://doi.org/10.1063/5.0225759>

## I. INTRODUCTION

The microscopic structure of amorphous systems has long been interpreted in terms of pairwise correlations, from the work of Ornstein and Zernike a century ago onward.<sup>1</sup> However, in the case of many phenomena, such as crystal nucleation<sup>2–4</sup> and the glass transition,<sup>5–8</sup> higher-order correlations in structure have been shown to be important. One way to tackle higher-order structure has its roots in the work of Sir Charles Frank who showed that the minimum energy cluster of 13 Lennard-Jones particles is an icosahedron. Frank inferred “that this will be a very common grouping in liquids.”<sup>5</sup>

It has since become possible to identify such icosahedra, and other geometric motifs, in bulk systems.<sup>9–11</sup> By identifying minimum energy clusters for certain model systems<sup>12,13</sup> and determining bonds in a bulk system, one may identify groups of particles whose bond topology is identical to that of isolated minimum energy clusters. Therefore, in addition to isolated clusters,<sup>14–18</sup> it is possible to identify geometric motifs, which might be expected to be significant in the bulk.<sup>10,19–21</sup> The significance of identifying higher-order

structure in the bulk is that it enables unique insights into the behavior of the system. For example, local structural motifs with fivefold symmetry (icosahedra) have long been thought to play a key role in the glass transition. Indeed, these underlie a leading theory of the glass transition, geometric frustration.<sup>6</sup> Icosahedra and related geometric motifs have since been shown to play a significant role in viscous liquids.<sup>8,9,11,22,23</sup> These geometric motifs are also implicated in the rigid network of colloidal gels.<sup>24,25</sup> Other examples of the use of such geometric motifs include an understanding of the mechanism of crystallization. This has been applied to crystal nucleation.<sup>3,4,26–29</sup> It has been possible to control crystallization through fivefold symmetric structures.<sup>26</sup>

So far, this sort of analysis has largely been restricted to particles with isotropic interactions. Of course, very many systems have particles that interact in an anisotropic manner, and so here, we make the first steps in developing the methodology of higher-order structure for this more general case. Among the simplest ways to introduce anisotropy is through a dipolar interaction. For example, the Stockmayer model combines a dipolar interaction with a Lennard-Jones potential,<sup>30</sup> and this way is a simple model for a molecule with a per-

manent dipole and magnetic nanoparticles.<sup>31</sup> In colloidal systems, dipolar interactions are often induced by an external AC electric field or magnetic field.<sup>32</sup> The phase behavior of these systems has been studied in experiment<sup>32–35</sup> and simulation.<sup>36</sup> At sufficient field strength, the particles organize into vertically oriented “strings.”<sup>33</sup> In addition to their fundamental interest, these *electro-rheological fluids* have potential applications as smart shock absorbers and clutches<sup>37</sup> as well as in photonic materials.<sup>38</sup>

Such dipolar colloids then form a suitable system with anisotropic interactions in which to consider higher-order structures. Therefore, we consider the minimum energy clusters of a basic model for dipolar colloids. Motivated by the comparable similarity of the higher-order structure of colloidal fluids (represented as hard spheres or particles with an effective attraction<sup>35</sup>) and Lennard-Jones liquids, in that the same clusters are found in both,<sup>13,19,20,39</sup> we consider a combination of a Lennard-Jones and dipolar interaction aligned along the  $z$  axis. That is to say, we consider the Stockmayer model modified, such that the dipolar contribution is aligned in  $z$ . Now, the minimum energy state of two dipolar particles is in alignment with the applied field. If we consider the case where more particles are added to the system, then at low dipole strengths, however, the energy of the isotropic interaction must at some point be comparable with the dipolar interaction. In a study of Stockmayer particles, Miller and Wales<sup>30</sup> discovered a rich family of clusters, with complex knots and rings occurring at low dipole strength, which forms a playground to study topological transitions.<sup>40</sup> Other more exotic possibilities include quadrupolar interactions,<sup>41</sup> which may potentially also be realized in colloidal systems.<sup>42</sup>

We have identified the minimum energy clusters of  $6 \leq m \leq 13$  particles for the case applicable to induced dipoles in an external field. This was achieved with the basin hopping algorithm implemented in the GMIN energy minimization package.<sup>13,43</sup> In all cases, we observe a string forming at high dipole strengths. The pathway to string assembly as the dipole strength is increased reveals a set of distinct clusters. We have characterized these structures as Lennard-Jones polytetrahedra, non-Lennard-Jones polytetrahedra (which tend to be stretched in the field direction), and clusters based on octahedra and Bernal spirals. We also find that as the field strength is increased further, non-rigid particles are found at high fields and finally strings are formed.

Each minimum energy cluster has a unique bond topology that can be identified by Voronoi decomposition. To characterize particle-resolved experimental and simulation data, we have implemented these new clusters into the *topological cluster classification*.<sup>10</sup> This is a computational tool, which identifies target clusters by their bond topology in bulk systems. This enables such minimum energy clusters to be identified in systems at high volume fraction. We finally demonstrate the validity of this approach with computer simulation results.

This work is organized as follows: in the methodology section (Sec. II), we first outline the energy minimization methods (Sec. II A) before briefly describing the topological cluster classification (Sec. II B) and finally the molecular dynamics simulations with which we test our implementation in Sec. II C. The results are presented in Sec. III. This is broken up into the results from the energy minimization (Sec. III A), followed by the implementation of the topological cluster classification (Sec. III B). This itself is divided into identification of stretched polytetrahedra (Sec. III B 1),

clusters based on the 6A octahedron (Sec. III B 2), and spiral clusters (Sec. III B 3). We then consider the results from the computer simulations in Sec. III C. Finally, we discuss our findings in Sec. IV and conclude in Sec. V.

## II. METHODS

### A. Energy minimization simulation

The system considered is a set of  $m$  particles interacting through the Stockmayer potential, where the dipoles are fixed parallel to the  $z$  axis. The interparticle interaction is thus defined as

$$\beta u_{\text{ldip}}(r, \theta) = 4\beta\epsilon \left[ \left( \frac{\sigma}{r} \right)^{12} - \left( \frac{\sigma}{r} \right)^6 \right] - \beta\mu^2 \frac{\sigma^3}{r^3} (1 - 3\cos^2\theta), \quad (1)$$

where  $\beta = 1/k_B T$  and  $\theta$  is the azimuthal angle between the two reduced dipole moments  $\mu$ . Here, we set the thermal energy to unity.

We consider clusters of size  $6 \leq m \leq 13$ . In fact, the topology of  $m = 6$  clusters is already accounted for by work on systems with spherically symmetric interactions, but we include these as there are two structures that are not strings.<sup>10</sup> Larger ( $m > 13$ ) clusters are, in principle, possible to calculate, but these are technically challenging to implement in the cluster search code, and the resulting search is rather slow. Moreover, the role of higher-order structure in dense amorphous systems, such as glassformers, appears to be largely dominated by clusters with a single shell around the central particle ( $m = 13$ ) and smaller clusters.<sup>8</sup> Other examples, such as crystal nucleation, also tend to invoke smaller clusters.<sup>28,44</sup>

The minimum energy cluster of each combination of  $m$  and  $\mu$  was explored using the GMIN energy minimization package. A modified version of the in-built Stockmayer potential was used. GMIN uses a “basin-hopping” algorithm to minimize the energy.<sup>13</sup> The basin-hopping algorithm randomly perturbs the coordinates and then performs an optimization that is rejected or accepted based on Monte Carlo criteria. This is repeated until a specified convergence criterion is met.

In the basin hopping, reduced units were used, with  $\epsilon$  and  $\sigma$  set to unity. The dipole strength was varied between 0 and 3. 25 000 basin-hopping steps were performed and temperature, which determines the Monte Carlo basin hopping threshold was held at 1.5. It should be noted that as in all energy minimization simulation, there can be no absolute assurance that these are the global minima, but for each value of  $\mu$  and  $m$ , the energy minimization was repeated ten times. Only the lowest energy clusters were considered. In the case of larger clusters ( $m = 12, 13$ ), for high field strengths, not all runs at the intersecting string-string transition converged to the same shape. This is presumably due to the large interaction strengths. However, our focus in this work is on the clusters rather than the intersecting strings or strings, so we neglect this here.

### B. Topological cluster classification

For a complete explanation of the topological cluster classification, Malins *et al.*<sup>10</sup> should be referred to. The topological cluster classification identifies target clusters by their bond network; these are polyhedra that are associated with a unique bond topology. The

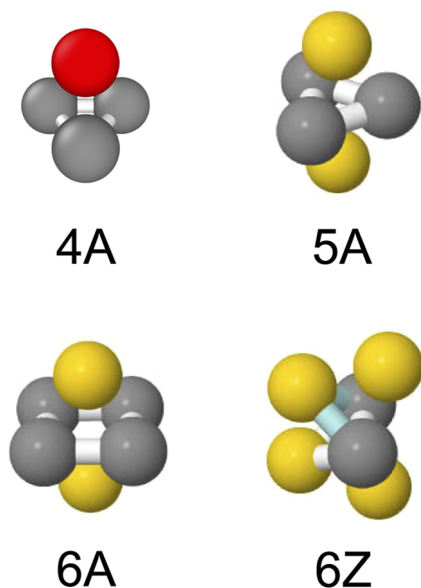


**FIG. 1.** 4A, 5A, 6A, and 6Z clusters. Gray indicates ring particles; yellow indicates spindle particles; and red indicates a single spindle particle.

bond network may be defined either with a distance criterion or with a Voronoi decomposition combined with a distance criterion. As the basic building block for clusters, the algorithm identifies all the three, four, and five-membered rings, which can be constructed along the bond network. Rigid structures are built by considering all the particles that are bonded to every member of each ring. From these small rigid clusters, larger and more complex shapes are built. Figure 1 shows the three basic clusters of interest here: the 4A (tetrahedron), 5A (triangular bipyramid), 6A (octahedron), and 6Z (polytetrahedron).<sup>45</sup> The gray particles indicate rings, and the yellow particles are spindles. Where a particle is both a ring and a spindle, they are colored for clarity. The bonds indicate rings. The red particles are bonded to three particles as part of a single-spindle 4A cluster (Fig. 1).

### C. Molecular dynamics computer simulation

We will show that in the Lennard-Jones dipolar system, a number of novel minimum energy clusters are found. Cluster populations are an important characteristic of colloidal fluids. In order to demonstrate the viability of these clusters as a characteristic of dipolar colloidal systems, we perform molecular dynamics computer simulations and use the topological cluster classification to identify the target clusters. Simulations were performed with the Large-scale Atomic/Molecular Massively Parallel Simulator (LAMMPS) molecular dynamics package<sup>46</sup> with Brownian dynamics time integration.<sup>47</sup>

Simulations are performed on a system of 512 particles, at an effective volume fraction of around 0.0509, with the effective hard sphere diameter determined with the Barker-Henderson method, where we consider the repulsive part of the interaction potential to define the hard core.<sup>1</sup> Simulations are carried out for the following values of the dipole strength:  $\mu = 0, 0.3, 0.6, 0.9, 1.2, 1.5, 1.8, 2.1, 2.4$ ,

and 2.7 (for each case, the dipole strength is constant throughout the simulation). The simulations are run for  $5 \times 10^8$  time steps with a time step of 0.000 01.

Now, the Lennard-Jones interaction can lead to bulk phase separation. It is known that adding a weak, long-ranged repulsion can stabilize clusters,<sup>48</sup> which interact with one another very weakly. Such weakly repulsive clusters have been realized on experiments in colloids and proteins.<sup>49,50</sup> The topology of such clusters, stabilized by long-ranged repulsions, has been investigated in simulation and experiment for systems with spherically symmetric interactions.<sup>14,51,52</sup> In that case, a sufficiently weak Yukawa repulsion was found not to perturb the cluster topology significantly, with respect to the case of isolated clusters without the repulsion.<sup>14,16,51</sup> Here, we apply the same principle of using a long-ranged repulsion to stabilize clusters to the Lennard-Jones dipolar system. To achieve this, we add a weak Yukawa potential to Eq. (1) of the form

$$\beta u_{\text{yuk}}(r) = -\beta A \frac{e^{-\kappa r}}{r/\sigma}, \quad (2)$$

where the prefactor  $A = 1$  and inverse screening length  $\kappa\sigma = 0.5$ . The simulations are then evolved according to  $\beta u_{\text{sim}}(r, \theta) = \beta u_{\text{LJdip}}(r, \theta) + \beta u_{\text{yuk}}(r)$ .

## III. RESULTS

### A. Minimum energy clusters of the fixed dipolar Lennard-Jones system

The change in topology of minimum energy clusters as the cluster size and dipole strength are varied may be represented as a “phase diagram” in the energy  $E$ –dipole strength  $\mu$  plane, as shown in Fig. 2. For all cluster sizes, at high dipole strengths, the minimum energy cluster is a string, and at low dipole strengths, with the minimum energy cluster, we recover the Lennard-Jones minima. For  $m = 6$ , the minimum energy Lennard-Jones cluster is the 6A octahedron (Fig. 1). For  $7 \leq m \leq 13$ , the minimum energy clusters are polytetrahedral and are denoted by 7A, 8B, 9B, 10B, 11C, 12B, and 13A<sup>13</sup> in the nomenclature of Doye, Wales, and Berry<sup>12</sup> and are shown in Fig. 13 in the Appendix for completeness. At high field strength, the particles form an interlocking string

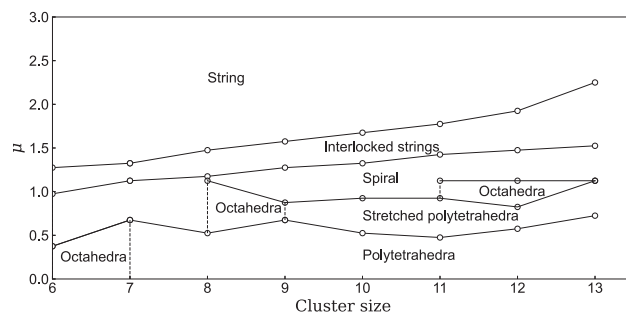


**FIG. 2.** Summary “phase diagram” of the clusters of Lennard-Jones particles, with a dipole whose direction is fixed in the  $z$  direction determined using GMIN. The dotted lines indicate the change of structure.

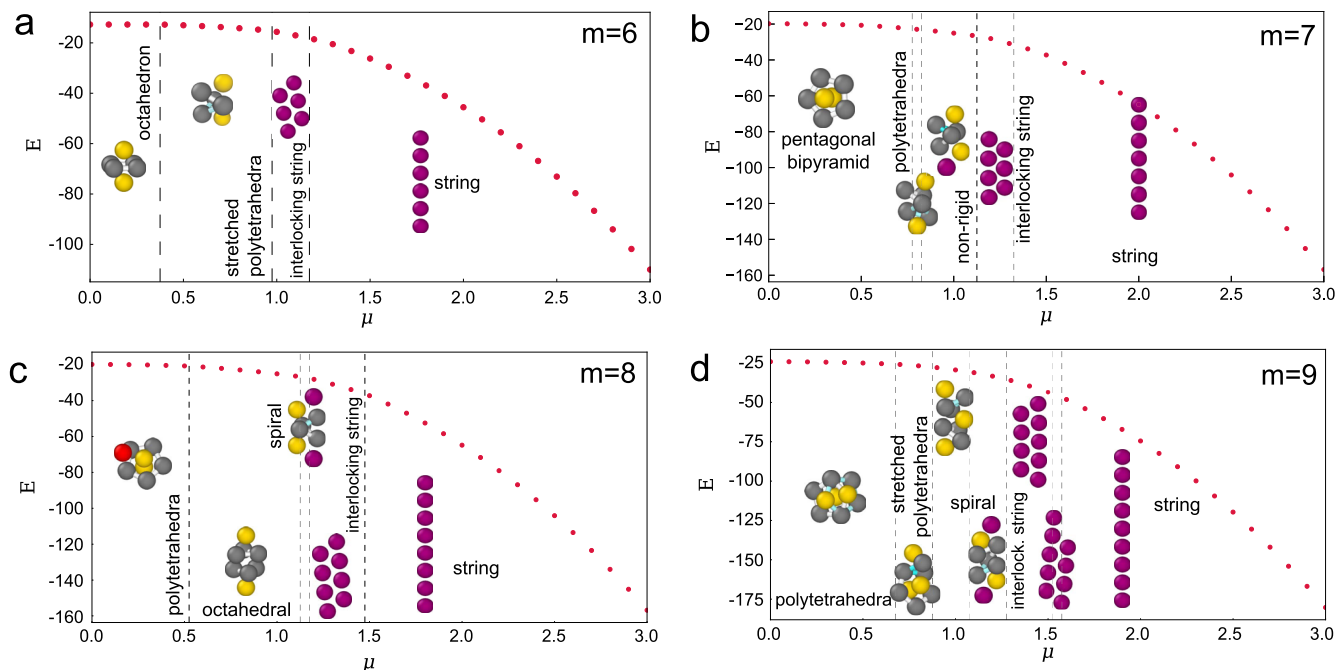


**FIG. 3.** Structural phase diagrams for clusters of size  $m = 6$  to  $m = 9$ . Representation of the minimum energy cluster of six to nine dipolar particles as a function of dipole strength  $\mu$  and their associated energy. The dashed lines indicate the change of structure. The dotted line is a best fit through the energy corresponding to each geometry.

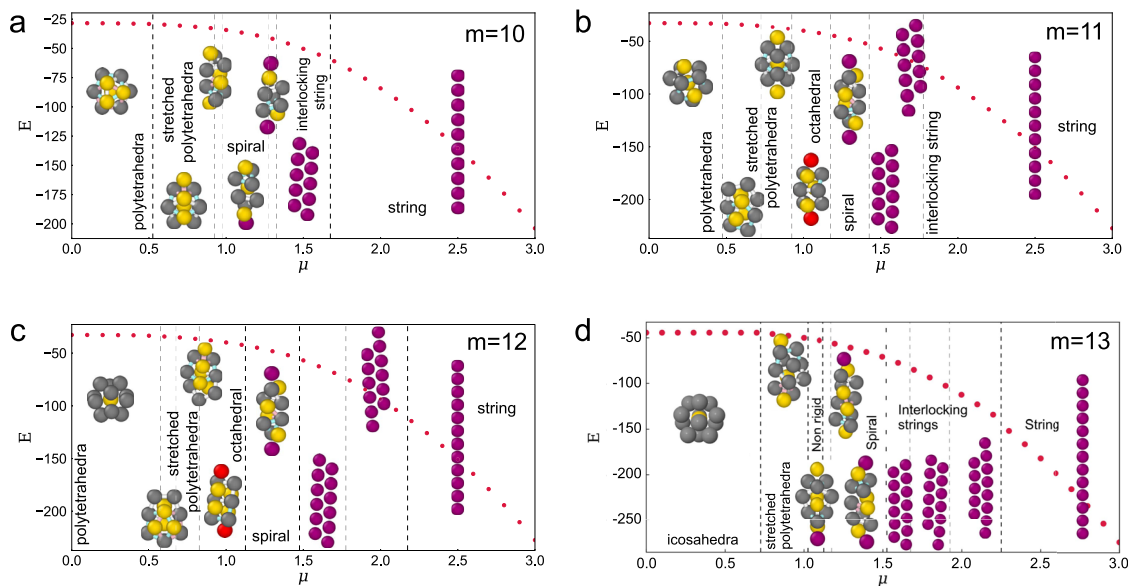


**FIG. 4.** Structural phase diagrams for clusters of size  $m = 10$  to  $m = 13$ . Representation of the minimum energy cluster of 10 to 13 dipolar particles as a function of dipole strength  $\mu$  and their associated energy. The dashed lines indicate the change of structure. The dotted line is a best fit through the energy corresponding to each geometry.

**TABLE I.** Detection routines for all the *rigid* minimum energy clusters of dipolar particles whose dipole is fixed with respect to an external axis. Here, “P” clusters are spiral, “S” clusters are polytetrahedral but “stretched” with respect to the Lennard-Jones clusters, and “O” clusters are based on 6A octahedra. The letters “AA” in the spiral cluster name indicate that both ends of the cluster are rigid; “AB” or “BB” would indicate that one or both ends were non rigid. Detection for the spiral clusters *mPAA*, *mPAB*, and *mPBB* is given in Sec. III B 3.

Cluster	Detection routine	Figures
8O	A 6Z cluster and two 4A clusters, where Each 4A cluster shares three particles with the 6Z and the two 4A clusters have no particles in common	6
9S	An 8B and a 5A, where The clusters share a spindle particle and two ring particles. The remaining ring particle of the 5A is the “additional” (not part of a 7A) particle of the 8B.	5
9PAA	Two 6Z clusters and one 5A cluster where: The 6Z clusters share a common spindle and two common ring particles. The remaining spindle of each 6Z cluster is a ring particle of the other. The 5A shares a common spindle particle with 6Z <sub>i</sub> . The 5A shares two ring particles with 6Z <sub>i</sub> . The remaining 5A ring particle is the remaining spindle 6Z <sub>i</sub> . All the particles in 5A and 6Z <sub>j</sub> are distinct	7
10S	A 7A and a 5A cluster where: The clusters have one common spindle particle and one common ring particle. The clusters have only two particles in common.	5
10PAA	Two 9PAA clusters which have eight particles in common	7
11S	Three 7A clusters where: 7A <sub>i</sub> and 7A <sub>j</sub> form a 9A. The ring of 7A <sub>k</sub> is the uncommon spindle of 7A <sub>j</sub> and an uncommon ring of 7A <sub>j</sub> . The ring particles of 7A <sub>k</sub> comprise the other uncommon ring of 7A <sub>j</sub> , The common spindle particles of 7A <sub>i</sub> and 7A <sub>j</sub> , one common ring particle of 7A <sub>i</sub> and 7A <sub>j</sub>	5
11SB	Two 7A and two 5A clusters, where 7A <sub>i</sub> and 7A <sub>j</sub> form a 9A and 5A <sub>i</sub> and 5A <sub>j</sub> have a common spindle. One ring particle of 5A <sub>ij</sub> is a spindle of 7A <sub>ij</sub> , and this spindle is not the 7A <sub>ij</sub> shared spindle. Two ring particles of 5A <sub>ij</sub> are ring particles of 7A <sub>ij</sub> , and these ring particles are not shared between 7A <sub>ij</sub> .	5
11O	Two 6A clusters and two sp3b clusters, where 6A <sub>i</sub> and 6A <sub>j</sub> have two particles in common. sp3b <sub>ij</sub> has three common particles with 6A <sub>ij</sub> and none with 6A <sub>ji</sub> . There is no sp3b <sub>k</sub> within 6A <sub>i</sub> and 6A <sub>j</sub> which has common particles with both sp3b <sub>i</sub> and sp3b <sub>j</sub> .	6
12S	Three 7A clusters, where 7A <sub>i</sub> and 7A <sub>j</sub> share 3 particles. 7A <sub>i</sub> and 7A <sub>k</sub> share 3 particles. 7A <sub>k</sub> and 7A <sub>j</sub> share four particles. 7A <sub>i</sub> has a spindle particle which is a ring of both 7A <sub>j</sub> and 7A <sub>k</sub> . 7A <sub>i</sub> has a ring particle which is a spindle of both 7A <sub>j</sub> and 7A <sub>k</sub> . Any two 7A have a common ring particle.	5
12SB	A 11SB and a 5A, where One spindle of the 5A is the common spindle particles of the two 7A clusters within the 11SB. Three particles of the 5A are common with one of the 7A clusters within the 11SB.	5
12O	Two 6Z and two sp3b clusters, where 6Z <sub>i</sub> and 6Z <sub>j</sub> share two particles. sp3b <sub>ij</sub> has three common particles with 6Z <sub>ij</sub> and none with 6Z <sub>ji</sub> . There is no sp3b <sub>k</sub> within 6A <sub>i</sub> and 6A <sub>j</sub> , which has common particles with both sp3b <sub>i</sub> and sp3b <sub>j</sub> .	6
13S	A 12SB and a 5A cluster, where One ring of the 5A is the “additional” (not part of an 11SB) particle of the 12SB. One ring of the 5A is an “additional” (not part of a 9B) particle of the 11SB within the 12SB. The remaining ring particle of the 5A is common with the 12SB.	5

two-particles thick, which transitions to a string one-particle thick upon further increase in the field. Between these regimes of Lennard-Jones clusters and strings, the intermediate clusters may be grouped as polytetrahedral, clusters based on 6A octahedra (Fig. 1), and spiral clusters.

Figures 3 and 4 show the full cluster “phase diagrams” for cluster sizes from 6 to 13 particles. As shown before in Fig. 1, the gray particles indicate rings and the yellow particles are spindles. Where a particle is both a ring and a spindle, they are colored for clarity. Bonds indicate rings where the color indicates the ring. The red particles are bonded to three particles as part of a single-spindle 4A cluster (Fig. 1). The purple particles are non-rigid.

## B. Identification of clusters with the topological cluster classification

Once the minimum energy clusters have been determined, we seek a means to identify them in bulk coordinate data, either in experiments or simulations. To this end, we have implemented the new clusters into the topological cluster classification. Table I presents the detection routines whereby each rigid cluster may be identified from simulation or experimental coordinate data. Figure 1 shows four structures, which are the building blocks of all the larger rigid clusters. We now describe the detection procedure for each geometry—stretched polytetrahedra, octahedra-based, and spiral clusters.

### 1. Non-Lennard-Jones “stretched” polytetrahedra

As the dipole strength is increased from zero, the first class of clusters are non-LJ polytetrahedra. The dipolar interaction acts to elongate the cluster, moving one or more particles from the sides of the cluster to the top or bottom. We denote these clusters by “S” due

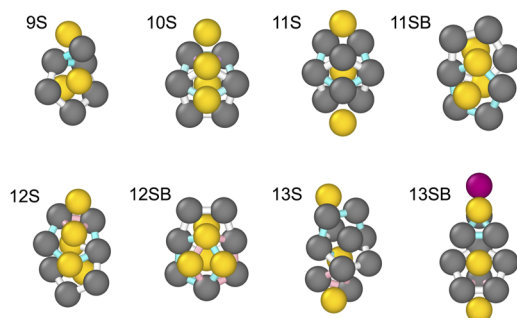


**FIG. 5.** Renderings of non-Lennard-Jones or “stretched” polytetrahedral clusters. For 9S, the five-membered ring is denoted with the white bonds and three-membered ring with the blue bonds. For 10S, the interlocking five-membered rings are indicated with the blue and white bonds. The three-membered ring toward the top of the cluster is indicated with the pink bonds. The two interlocking five-membered rings of 11S and 11SB are shown in the blue and white bonds. In the case of 12S, the 2 five-membered rings are indicated in blue and white and the three-membered ring is shown in pink. For 12SB, the 3 five-membered rings are indicated in white, blue, and pink. For 13S, the interlocking five-membered rings are shown in blue and white. The 13SB has a three-membered ring (blue) and a five-membered ring (white).

to their stretching with respect to the  $\mu = 0$  case. For  $m \geq 11$ , there is more than one polytetrahedral minimum before the system transitions to the spiral or octahedral cluster. These clusters are shown in Fig. 5.

The 9S and 10S clusters are formed by taking the Lennard-Jones cluster for eight or nine particles and adding an additional particle such that this particle forms a 5A triangular bipyramid, which points in the direction of the field. The 11S and 12S clusters are formed from two and three intersecting 7A pentagonal bipyramids, which are stacked such that the cluster is elongated parallel to the field. The 11SB cluster is formed from the 9A cluster with two additional particles, each forming a 5A at either end of the cluster. The 12SB cluster is formed from an 11S cluster with an additional particle added to form a 5A aligned with the dipoles. The 13S cluster is formed from a 12SB cluster with an additional particle forming a 5A. Finally, the 13SB is a 12S with an additional particle forming a three-membered ring. 13SB is the only non-rigid cluster that is not a spiral, an interlocked string, or a string.

### 2. Octahedra-based clusters

For  $m = 8$ ,  $m = 11$ , and  $m = 12$ , there is no point where the energy minimum is the non-rigid  $m$ PAB spiral (see Sec. III B 3); instead, between the non-LJ polytetrahedra and the  $m$ PBB non-rigid spiral, the energy minimum cluster is based on the 6A octahedron. We, therefore, denote these clusters as “O.” 8O, 11O, and 12O (see Fig. 6). These clusters are intersections between 6A octahedra and 4A tetrahedra (see Table I).

8O is formed from a 6A cluster and two 4A clusters. 11O is formed by two intersecting 6A clusters, which share two rings and one spindle particle. The remaining spindle and ring of each 6A form a 4A cluster with one additional particle. 12O is also formed from two 6A and two 4A clusters; however, here the 6A clusters share two ring particles but no spindles. 11O and 12O, therefore, represent two types of octahedral clusters differentiated by the number of particles shared by the 6A. The next largest octahedral clusters of type 11O would be 14O, 17O, and 21O. The next largest clusters of type 12O would be 16O, 20O, and 24O. The study of these larger octahedral clusters would be a useful target for future research, subject to the caveats noted above.

### 3. Spiral clusters

For each cluster size studied, there is a range of values of dipolar strength  $\mu$ , where the minimum energy cluster is a spiral. For each value of  $m$ , there are three spirals denoted PAA, PAB, and PBB;

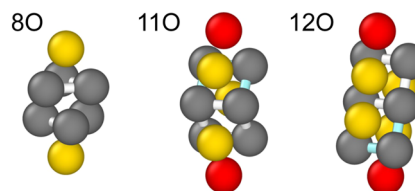


**FIG. 6.** Renderings of clusters based on the 6A octahedron. The 2 three-membered rings are rendered with white bonds in the 8O cluster. For 11O, the 2 four-membered rings are indicated with white and blue bonds. For the 12O, the four-membered rings are shown in blue and white.

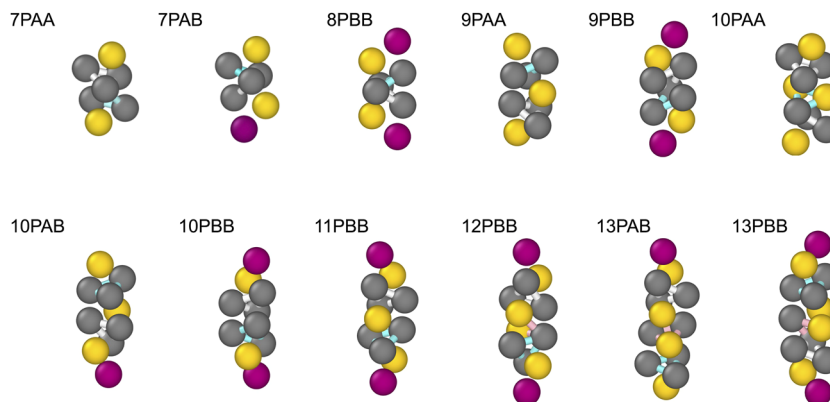


**FIG. 7.** Renderings of spiral clusters. For 7PAA, 7PAB, 8PBB, 9PAA, and 9PBB, the 2 three-membered rings are indicated by the blue and white bonds. In the case of 10PAA, the 3 three-membered rings are indicated by the blue and white bonds. For 10PAB and 10PBB, the 2 three-membered rings are indicated by the blue and white bonds. For 11PBB, the 2 three-membered rings are indicated by the white and blue bonds. The 12PBB has 3 three-membered rings indicated by the white, pink, and blue bonds. For 13PAB and 13PBB, the 3 three-membered rings are indicated by the pink, white, and blue bonds.

however, only for  $m = 10$  are all three clusters an energy minima for some value of  $\mu$ . As shown in Fig. 7, the basin-hopping simulations have identified the following clusters as energy minima for some value of  $\mu$ : 7PAA, 7PAB, 8PAB, 9PAA, 9PBB, 10PAA, 10PAB, 10PBB, 11PBB, 12PBB, and 13PAB. The  $m$ PAA are fully rigid;  $m$ PAB have one non-rigid particle (purple in Fig. 7); and  $m$ PBB have two non-rigid particles. We note that for  $N = 8, 11$ , and  $12$ , the octahedral cluster would appear to replace the PAB cluster. Having a helical structure, the spiral clusters are chiral. The basin-hopping output both right- and left-handed spirals. These have the same energy, and the TCC search algorithm does not differentiate between them.

We will first consider the rigid spirals 9PAA and 10PAA. The spiral  $m$ PAA cluster is comprised of  $m - 5$  intersecting 6Z clusters. 6Z is the minimum energy cluster of six particles interacting through the Dzugutov potential and the Lennard-Jones–dipolar interaction for suitable values of  $\mu$  [Fig. 3(a)]. Since 6Z is itself two intersecting 5A clusters, the spirals may equally be considered intersecting 5A. Figure 8 shows the labeled particles in a 6Z cluster. To be considered 6Z, the two 5A clusters must intersect

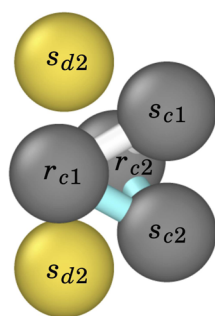


**FIG. 8.** 6Z cluster with labeled particles. See the text for the interpretation of the labels.

such that they share two ring particles  $rc1$  and  $rc2$ . The remaining ring particle of each cluster must be a spindle particle of the other  $sc1$  and  $sc2$ . The final two spindles are denoted as  $sd1$  and  $sd2$ .

Figure 9 shows the constituent 5A and 6Z clusters for 10PAA. If one particle is removed from either end of 10PAA, we have a 9PAA cluster comprised of four intersecting 6Z or five intersecting 5A. A 10PAA cluster adds another particle to this 9PAA, such that the additional particle forms a spindle of another intersecting 5A cluster. This new 5A cluster must intersect with the lower or upper 5A cluster such that a new 6Z cluster is formed (Fig. 10).

To build larger spirals, this same routine is performed at the ends of the spiral. In a 6Z cluster, there are only two 5A clusters, but for larger spirals, there will be more; only the 5A clusters at the top and bottom of the cluster can grow the cluster by forming a new 6Z. Therefore, in the implementation of the topological cluster classification, each particle must be assigned its own index.

The other class of spiral clusters is the non-rigid. In these clusters, an additional particle is added to a spiral, which is bonded in a three-membered ring to the non-shared spindle and the non-shared ring particle of the outermost 6A. In the implementation of the topological cluster classification, this third particle must have only two bonds to the existing cluster.

### C. Results from molecular dynamics simulations

The populations of all the minimum energy clusters obtained from the molecular dynamics simulations performed, as described in Sec. II C, will now be considered for various values of the dipole strength  $\mu$ . Snapshots are shown in Fig. 11 for certain values of  $\mu$ . We emphasize that our purpose here is to provide a demonstration of the use of the topological cluster classification for the Lennard-Jones–dipolar system that we have developed, rather than to carry out an exhaustive study.



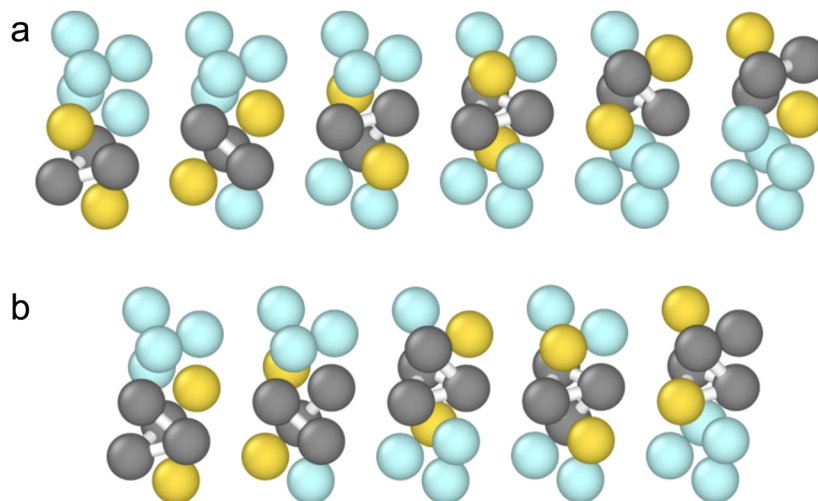


FIG. 9. Building the 10PAA cluster from (a) six intersecting 5A or equivalently (b) five intersecting 6A clusters.

The results shown in Fig. 12 show the populations of all the clusters, grouped by size, as a function of  $\mu$ . This shows that the populations of the different classes of clusters show qualitative agreement with the transitions shown in Sec. III B 3. At low dipole strengths, the populations of Lennard-Jones clusters are highest. The populations of the non-LJ stretched polytetrahedra are also higher at the low dipole strengths, and in the cases of  $m = 10, 11, 12$ , and 13, the non-LJ polytetrahedra persist to higher field strengths than the Lennard-Jones clusters. The results show that the peak in the population of the 8O and 12O octahedra-based clusters is found at intermediate field strengths. These clusters are both observed within larger octahedral columnar structures. The absence of the 11O cluster is suggested as an avenue for future research. Finally, the populations of smaller spiral clusters 7PAA, 7PAB, and 9PBB peak at  $\mu \approx 1$ . This is at a higher value of  $\mu$  than the octahedral clusters, which is qualitatively consistent with the transition found in the basin-hopping simulations. It may be expected that for larger clusters, the transitions shift to higher values of  $\mu$ . Therefore, while the peaks in octahedral, non-LJ polytetrahedra, and spiral clusters are at higher values of  $\mu$  than in the GMIN simulation results, these still support a transition from Lennard-Jones to non-LJ polytetrahedra to octahedra-based to spirals as the dipole strength is increased. The

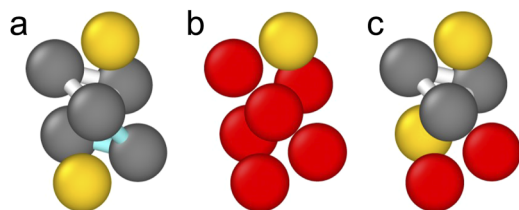


FIG. 10. Adding particles to grow a spiral 7PAA cluster from a 6Z cluster. Panel (a) shows 7PAA as two intersecting 5A clusters. Panel (b) shows the 6Z cluster and the additional particle. Panel (c) shows how the additional particle forms 5A with the original 6Z cluster.

results also imply that the order of these transitions would hold for larger clusters.

#### IV. DISCUSSION

In determining its minimum energy clusters and implementing these in the topological cluster classification, we introduce the ability to carry out higher-order structural analysis for the dipolar colloidal system. This opens a range of new materials, which can now be studied with this methodology. For example, helical structures at the

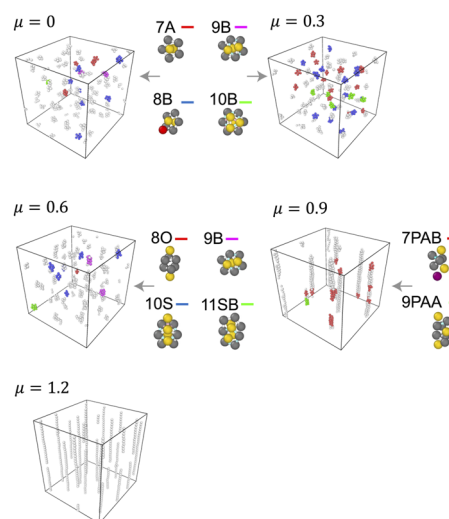


FIG. 11. Rendering of molecular dynamics simulation, with corresponding minimum energy clusters shown. These snapshots were taken at the end of the run, i.e., after  $5 \times 10^3$  time units. The colors of the particles correspond to the lines by the clusters depicted to the right of the snapshots.

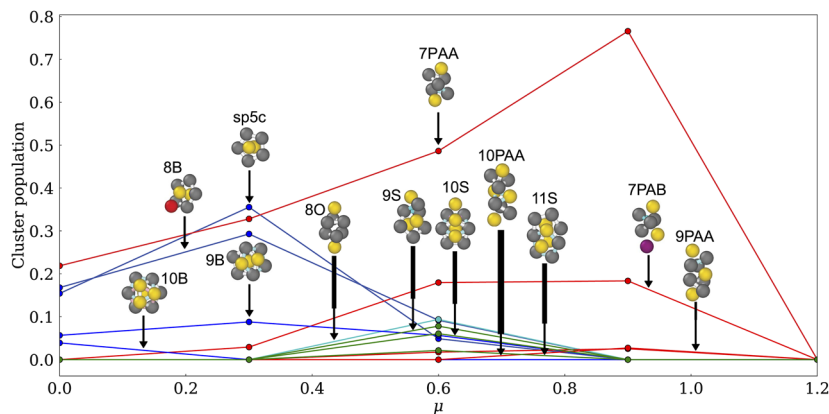


FIG. 12. Population of clusters as a function of dipole strength in molecular dynamics simulation data.

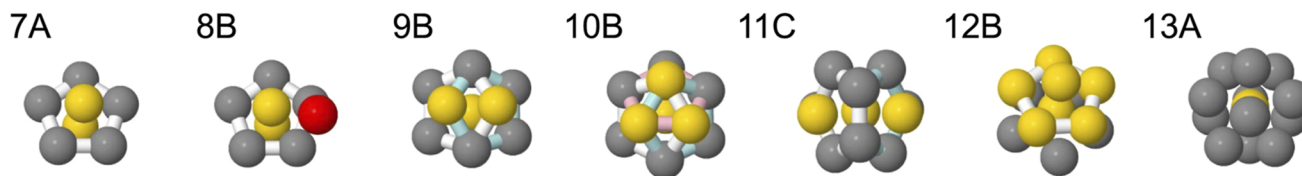


FIG. 13. Lennard-Jones minimum energy clusters, determined by Wales and Doye.<sup>13</sup> These have been previously implemented in the TCC.<sup>10</sup>

microscale and nanoscale have been suggested as promising structures in opto-electronics<sup>53</sup> and catalysis,<sup>54</sup> and they have potential for understanding chiral structure in biopolymers.<sup>55,56</sup> The assembly of Bernal spirals is also seen in systems of patchy colloids.<sup>57,58</sup> In addition, string structures comprised of stacking tetrahedra have also been observed in polarized, metalodielectric Janus particles<sup>59,60</sup> and notably the active colloidal dipolar system.<sup>61</sup> The observation of helical structures in the potential energy landscape is, therefore, of importance to a wide range of systems. It is quite possible that many of the same structures that we have identified here would be found in these systems, which would be interesting to explore in the future.

In addition to these systems with anisotropic interactions, some of the clusters that we have identified here have, in fact, also been observed in systems with *isotropic* interactions. In particular, so-called short-range attraction long-range repulsion or SALR particles<sup>50</sup> have been shown to form Bernal spirals.<sup>62</sup> Indeed, these are consistent with minimum energy clusters determined for the SALR potential.<sup>52</sup> In the future, it would be an interesting extension of this work to investigate the effect of weak repulsions in perturbing the clusters from isotropic Lennard-Jones minima, along with the other systems anisotropic interactions that we have mentioned here.

While the computer simulations that we have carried out merely serve as a proof-of-principle of the method we have implemented, we nevertheless take the liberty to make a few comments. As noted, the overall trends are very much in agreement with the expectation of Lennard-Jones polytetrahedra, stretched polytetrahedra, octahedra-based, spiral clusters, and strings as a function of dipolar

strength. However in the future, simulations that explicitly test the predictions of the GMIN calculations, in the precise Lennard-Jones–dipolar interactions (without the Yukawa contribution that we used here) would be desirable. These could, for example, form a model to explore kinetic trapping in an anisotropic system. For example, in comparison with simulations that considered a system with spherically symmetric interaction,<sup>51</sup> there appear to be a rather larger number of particles not identified in a minimum energy cluster. Whether this is due to geometric frustration<sup>14</sup> or some other cause would be an interesting avenue for future research.

## V. CONCLUSION AND OUTLOOK

We have identified a library of minimum energy clusters of particles with a Lennard-Jones interaction with a dipole fixed in one direction. We consider cluster sizes  $6 \leq m \leq 13$ . This model is relevant to colloidal systems in which dipolar interactions are induced by an electric field. These turn out to exhibit a rich structural “phase diagram” with a variety of topologies. As the dipolar strength is increased, the clusters transition from (relatively) isotropic polytetrahedra, which are minimum energy clusters of the Lennard-Jones model; these transition to “stretched” polytetrahedra, clusters based on octahedra, to Bernal spirals, to interlocking, before finally forming strings at high dipole strength.

We have implemented a search for these clusters in the topological cluster classification.<sup>10</sup> Since the TCC uses bulk coordinate data as its input, it is possible to investigate high-volume fraction systems. This marks a step forward in being able to use this kind of analysis of higher-order structure previously applicable

only to systems with isotropic interactions to anisotropic interactions. For example, insights into the mechanism of the glass transition,<sup>8,9,11,22,23</sup> gelation<sup>24,25</sup> and crystallization<sup>3,4,26–29</sup> are now possible for these dipolar particles, and may be extended to other systems with anisotropic interactions in the future. Finally, we provide an example of such analysis with a molecular dynamics simulation for a system of clusters whose interactions are very similar to the Lennard-Jones–dipolar interaction. We see a progression from isotropic Lennard-Jones clusters through the sequence of geometries to strings.

## ACKNOWLEDGMENTS

K.S. acknowledges the EPSRC doctoral training program for support. C.P.R. acknowledges the Agence Nationale de Recherche for grant DiViNew. F.J.M. was supported by a studentship provided by the Bristol Centre for Functional Nanomaterials (EPSRC Grant No. EP/L016648/1). The authors thank Mark Miller, Josh Robinson, and Peter Crowther for their help in building TCC software.

## AUTHOR DECLARATIONS

### Conflict of Interest

The authors have no conflicts to disclose.

### Author Contributions

**Katherine Skipper:** Conceptualization (equal); Data curation (equal); Formal analysis (equal); Investigation (equal); Methodology (equal); Resources (equal); Software (equal); Validation (equal); Visualization (equal); Writing – original draft (equal); Writing – review & editing (equal). **Fergus J. Moore:** Methodology (equal); Software (equal). **C. Patrick Royall:** Conceptualization (equal); Data curation (equal); Formal analysis (equal); Funding acquisition (equal); Investigation (equal); Methodology (equal); Project administration (equal); Resources (equal); Software (equal); Supervision (equal); Validation (equal); Writing – original draft (equal); Writing – review & editing (equal).

## DATA AVAILABILITY

The data that support the findings of this study are available from the corresponding author upon reasonable request.

## APPENDIX: LENNARD-JONES CLUSTERS

Lennard-Jones minimum energy clusters, determined by Wales and Doye, are shown in Fig. 13.

## REFERENCES

- J. Hansen and I. McDonald, *Theory of Simple Liquids: With Applications to Soft Matter* (Elsevier Science, 2013).
- C. P. Royall, P. Charbonneau, M. Dijkstra, J. Russo, F. Smallenburg, T. Speck, and C. Valeriani, “Colloidal hard spheres: Triumphs, challenges and mysteries,” *Rev. Mod. Phys.* (accepted) (2023); [arXiv:2305.02452](https://arxiv.org/abs/2305.02452).
- T. Kawasaki and H. Tanaka, “Formation of a crystal nucleus from liquid,” *Proc. Natl. Acad. Sci. U. S. A.* **107**, 14036–14041 (2010).

- J. Russo and H. Tanaka, “The microscopic pathway to crystallization in supercooled liquids,” *Sci. Rep.* **2**, 505 (2012).
- F. C. Frank, “Supercooling of liquids,” *Proc. R. Soc. London, Ser. A* **215**, 43–46 (1952).
- G. Tarjus, S. A. Kivelson, Z. Nussinov, and P. Viot, “The frustration-based approach of supercooled liquids and the glass transition: A review and critical assessment,” *J. Phys.: Condens. Matter* **17**, R1143–R1182 (2005).
- B. Charbonneau, P. Charbonneau, and G. Tarjus, “Geometrical frustration and static correlations in a simple glass former,” *Phys. Rev. Lett.* **108**, 035701 (2012).
- C. P. Royall and S. R. Williams, “The role of local structure in dynamical arrest,” *Phys. Rep.* **560**, 1–75 (2015).
- D. Coslovich and G. Pastore, “Understanding fragility in supercooled Lennard-Jones mixtures. I. Locally preferred structures,” *J. Chem. Phys.* **127**, 124504 (2007).
- A. Malins, S. Williams, J. Eggers, and C. Royall, “Identification of structure in condensed matter with the topological cluster classification,” *J. Chem. Phys.* **139**, 234506 (2013).
- H. Tanaka, H. Tong, R. Shi, and J. Russo, “Revealing key structural features hidden in liquids and glasses,” *Nat. Rev. Phys.* **1**, 333–348 (2019).
- J. P. K. Doye, D. J. Wales, and R. S. Berry, “The effect of the range of the potential on the structures of clusters,” *J. Chem. Phys.* **103**, 4234–4249 (1995).
- D. J. Wales and J. P. K. Doye, “Global optimization by basin-hopping and the lowest energy structures of Lennard-Jones clusters containing up to 110 atoms,” *J. Phys. Chem. A* **101**, 5111–5116 (1997).
- A. Malins, S. R. Williams, J. Eggers, H. Tanaka, and C. P. Royall, “Geometric frustration in small colloidal clusters,” *J. Phys.: Condens. Matter* **21**, 425103 (2009).
- G. Meng, N. Arkus, M. P. Brenner, and V. N. Manoharan, “The free-energy landscape of clusters of attractive hard spheres,” *Science* **327**, 560–563 (2010).
- C. L. Klix, K. Murata, H. Tanaka, S. R. Williams, A. Malins, and C. P. Royall, “Novel kinetic trapping in charged colloidal clusters due to self-induced surface charge organization,” *Sci. Rep.* **3**, 2072 (2013).
- V. N. Manoharan, “Colloidal matter: Packing, geometry, and entropy,” *Science* **349**, 1253751 (2015).
- L. Trombach, R. S. Hoy, D. J. Wales, and P. Schwerdtfeger, “From sticky-hard-sphere to Lennard-Jones-type clusters,” *Phys. Rev. E* **97**, 043309 (2018).
- J. Taffs, A. Malins, S. R. Williams, and C. P. Royall, “The effect of attractions on the local structure of liquids and colloidal fluids,” *J. Chem. Phys.* **133**, 244901 (2010).
- J. Taffs, A. Malins, S. R. Williams, and C. P. Royall, “A structural comparison of models of colloid-polymer mixtures,” *J. Phys.: Condens. Matter* **22**, 104119 (2010).
- A. Malins, J. Eggers, and C. P. Royall, “Investigating isomorphs with the topological cluster classification,” *J. Chem. Phys.* **139**, 234505 (2013).
- F. Turci, G. Tarjus, and C. P. Royall, “From glass formation to icosahedral ordering by curving three-dimensional space,” *Phys. Rev. Lett.* **118**, 215501 (2017).
- C. P. Royall and W. Kob, “Locally favoured structures and dynamic length scales in a simple glass-former,” *J. Stat. Mech.: Theory Exp.* **2017**, 024001.
- C. P. Royall, M. A. Faers, S. L. Fussell, and J. Hallett, “Real space analysis of colloidal gels: Triumphs, challenges and future directions,” *J. Phys.: Condens. Matter* **33**, 453002 (2021).
- D. Richard, J. E. Hallet, T. Speck, and C. Patrick Royall, “Coupling between criticality and gelation in “sticky” spheres: A structural analysis,” *Soft Matter* **14**, 5539–5694 (2018).
- J. Taffs and C. P. Royall, “The role of fivefold symmetry in suppressing crystallization,” *Nature Commun.* **7**, 13225 (2016).
- J. Taffs, S. R. Williams, H. Tanaka, and C. P. Royall, “Structure and kinetics in the freezing of nearly hard spheres,” *Soft Matter* **9**, 297–305 (2013); [arXiv:1206.5526](https://arxiv.org/abs/1206.5526).
- W. Gispen, G. M. Coli, R. van Damme, C. P. Royall, and M. Dijkstra, “Crystal polymorph selection mechanism of hard spheres hidden in the fluid,” *ACS Nano* **17**, 8807–8814 (2023).

- <sup>29</sup>G. Fiorucci, G. M. Coli, J. T. Padding, and M. Dijkstra, "The effect of hydrodynamics on the crystal nucleation of nearly hard spheres," *J. Chem. Phys.* **152**, 064903 (2020).
- <sup>30</sup>M. A. Miller and D. J. Wales, "Novel structural motifs in clusters of dipolar spheres: Knots, links, and coils," *J. Phys. Chem. B* **109**(49), 23109–23112 (2005).
- <sup>31</sup>M. A. Boles, M. Engel, and D. V. Talapin, "Self-assembly of colloidal nanocrystals: From intricate structures to functional materials," *Chem. Rev.* **116**, 11220–11289 (2016).
- <sup>32</sup>A. Ivlev, H. Löwen, G. E. Morfill, and C. P. Royall, *Complex Plasmas and Colloidal Dispersions: Particle-Resolved Studies of Classical Liquids and Solids* (World Scientific Publishing Co., Singapore, 2012).
- <sup>33</sup>A. Yethiraj and A. van Blaaderen, "A colloidal model system with an interaction tunable from hard sphere to soft and dipolar," *Nature* **421**, 513–517 (2003).
- <sup>34</sup>T. Colla, P. S. Mohanty, S. Nöjd, E. Bialik, A. Riede, P. Schurtenberger, and C. N. Likos, "Self-assembly of ionic microgels driven by an alternating electric field: Theory, simulations, and experiments," *ACS Nano* **12**, 4321 (2018).
- <sup>35</sup>S. Semwal, C. Clowe-Coish, I. Saika-Voivod, and A. Yethiraj, "Tunable colloids with dipolar and depletion interactions: Toward field-switchable crystals and gels," *Phys. Rev. X* **12**, 041021 (2022).
- <sup>36</sup>A.-P. Hynninen and M. Dijkstra, "Phase diagram of dipolar hard and soft spheres: Manipulation of colloidal crystal structures by an external field," *Phys. Rev. Lett.* **94**, 138303 (2005).
- <sup>37</sup>M. Parthasarathy and D. J. Klingenberg, "Electrorheology: Mechanisms and models," *Mater. Sci. Eng., R* **17**, 57–103 (1996).
- <sup>38</sup>A. van Blaaderen, "Colloids under external control," *MRS Bull.* **29**, 85–90 (2004).
- <sup>39</sup>J. F. Robinson, F. Turci, R. Roth, and C. P. Royall, "Morphometric approach to many-body correlations in hard spheres," *Phys. Rev. Lett.* **122**, 068004 (2019).
- <sup>40</sup>J. D. Farrell, C. Lines, J. Shepherd, D. Chakrabarti, M. A. Miller, and D. J. Wales, "Energy landscapes, structural topologies and rearrangement mechanisms in clusters of dipolar particles," *Soft Matter* **9**, 5407–5416 (2013).
- <sup>41</sup>M. A. Miller, J. J. Shepherd, and D. J. Wales, "Structural trends in clusters of quadrupolar spheres," *Mol. Phys.* **106**, 1655–1664 (2008).
- <sup>42</sup>J. E. Martin, R. A. Anderson, and C. P. Tigges, "Thermal coarsening of uniaxial and biaxial field-structured composites," *J. Chem. Phys.* **110**, 4854–4866 (1999).
- <sup>43</sup>Gmin: A program for finding global minima and calculating thermodynamic properties from basin-sampling.
- <sup>44</sup>N. Wood, J. Russo, F. Turci, and C. P. Royall, "Coupling of sedimentation and liquid structure: Influence on hard sphere nucleation," *J. Chem. Phys.* **149**, 204506 (2018).
- <sup>45</sup>Note that these differ from the basic clusters used in the previous version of the TCC<sup>10</sup>.
- <sup>46</sup>S. Plimpton, "Fast parallel algorithms for short-range molecular dynamics," *J. Comput. Phys.* **117**, 1–19 (1995).
- <sup>47</sup>F. J. Moore, J. Russo, T. B. Liverpool, and C. P. Royall, "Active Brownian particles in random and porous environments," *J. Chem. Phys.* **158**, 104907 (2023).
- <sup>48</sup>Y. Zhuang, K. Zhang, and P. Charbonneau, "Equilibrium phase behavior of a continuous-space microphase former," *Phys. Rev. Lett.* **116**, 098301 (2016).
- <sup>49</sup>A. Stradner, H. Sedgwick, F. Cardinaux, W.-C. Poon, S. Egelhaaf, and P. Schurtenberger, "Equilibrium cluster formation in concentrated protein solutions and colloids," *Nature* **432**, 492–495 (2004).
- <sup>50</sup>C. P. Royall, "Hunting mermaids in real space: Known knowns, known unknowns and unknown unknowns," *Soft Matter* **14**, 4020–4028 (2018).
- <sup>51</sup>A. Malins, S. R. Williams, J. Eggers, H. Tanaka, and C. P. Royall, "The effect of inter-cluster interactions on the structure of colloidal clusters," *J. Non-Cryst. Solids* **357**, 760–766 (2011).
- <sup>52</sup>S. Mossa, F. Sciortino, P. Tartaglia, and E. Zaccarelli, "Ground-state clusters for short-range attractive and long-range repulsive potentials," *Langmuir* **20**, 10756–10763 (2004).
- <sup>53</sup>B. Rosen, M. Peterca, K. Morimitsu, A. Dulcey, P. Leowanawat, A.-M. Resmerita, M. Imam, and V. Percec, "Programming the supramolecular helical polymerization of dendritic dipeptides via the stereochemical information of the dipeptide," *J. Am. Chem. Soc.* **133**, 5135–5151 (2011).
- <sup>54</sup>T. E. Gier, X. Bu, P. Feng, and G. D. Stucky, "Synthesis and organization of zeolite-like materials with three-dimensional helical pores," *Nature* **395**, 154–157 (1998).
- <sup>55</sup>D. Pijper and B. L. Feringa, "Control of dynamic helicity at the macro- and supramolecular level," *Soft Matter* **4**, 1349–1372 (2008).
- <sup>56</sup>E. Yashima, K. Maeda, H. Iida, Y. Furusho, and K. Nagai, "Helical polymers: Synthesis, structures, and functions," *Chem. Rev.* **109**, 6102–6211 (2009).
- <sup>57</sup>J. Morgan, D. Chakrabarti, N. Dorsaz, and D. Wales, "Designing a bernal spiral from patchy colloids," *ACS Nano* **7**, 1246 (2013).
- <sup>58</sup>S. N. Fejer, D. Chakrabarti, H. Kusumaatmaja, and D. J. Wales, "Design principles for bernal spirals and helices with tunable pitch," *Nanoscale* **6**, 9448–9456 (2014).
- <sup>59</sup>S. Gangwal, O. Cayre, and O. Velev, "Dielectrophoretic assembly of metal-dielectric Janus particles in ac electric fields," *Langmuir* **24**, 13312–13320 (2008).
- <sup>60</sup>L. Hong, A. Cacciuto, E. Luijten, and S. Granick, "Clusters of amphiphilic colloidal spheres," *Langmuir* **24**, 621–625 (2008).
- <sup>61</sup>N. Sakaï and C. P. Royall, "Active dipolar colloids in three dimensions: Strings, sheets, labyrinthine textures and crystals," [arXiv:2010.03925](https://arxiv.org/abs/2010.03925) (2020).
- <sup>62</sup>A. Campbell, V. Anderson, J. van Duijneveldt, and P. Bartlett, "Dynamical arrest in attractive colloids: The effect of long-range repulsion," *Phys. Rev. Lett.* **94**, 208301 (2005).